Optical Materials 34 (2012) 781–785

Contents lists available at SciVerse ScienceDirect

Optical Materials

journal homepage: www.elsevier.com/locate/optmat

Refractive index measurement of cerium-doped $Lu_xY_{2-x}SiO_5$ single crystal

Gábor Erdei [a], Noémi Berze [a], Ágnes Péter [b], Balázs Játékos [a], Emőke Lőrincz [a,*]

[a] Budapest University of Technology and Economics, Department of Atomic Physics, Budafoki 8, H-1111 Budapest, Hungary
[b] Research Institute for Solid State Physics and Optics, HAS, Konkoly Thege út 29-33, H-1121 Budapest, Hungary

ARTICLE INFO

Article history:
Received 19 January 2011
Received in revised form 18 October 2011
Accepted 5 November 2011
Available online 5 December 2011

Keywords:
Lutetium yttrium oxyorthosilicates
Refractive index
Scintillator
Axial dispersion

ABSTRACT

Principal refractive indices of the biaxial cerium-doped $Lu_xY_{2-x}SiO_5$ (LYSO) crystal were determined with high accuracy at seven different wavelengths between 400 and 700 nm using the classical minimum angle of deviation method. The reliability of the measured data permitted to deduce parameters of a common dispersion formula, by which the refractive indices can be extrapolated for wavelengths up to 1100 nm, an important range for laser applications. The extent of axial dispersion was precisely measured by ellipsometry, its effects on the anisotropic refractive index has been calculated. Examples are given to demonstrate the influence of anisotropy on the operation of optical devices.

1. Introduction

Rare-earth oxyorthosilicate (RE_2SiO_5, RE = Lu, Gd and Y) compounds are subject to growing interest: their low crystal symmetry and various forms of distorted substitutional sites make them a valuable alternative host to incorporate different types of dopants. For example, cerium-doped Lu_2SiO_5 (LSO), Y_2SiO_5 (YSO) and Gd_2SiO_5 (GSO) are commonly used as scintillators due to their high light yield and short scintillation decay time [1]. These crystals can also contain other rare-earth ions (Nd, Er, Yb, Ho and Pr) [2], offering new active media for laser amplifiers [3]. High-power femtosecond laser oscillations of ytterbium-doped silicates such as Yb:Y_2SiO_5 (Yb:YSO), Yb:Lu_2SiO_5 (Yb:LSO) and Yb:Gd_2SiO_5 (Yb:GSO) have already been demonstrated [4,5].

RE_2SiO_5 compounds are polymorphic: depending on the radius of RE^{3+} ions they crystallize in monoclinic structure type *P2/c*, (GSO) or *C2/c* (LSO, YSO) [6]. GSO, YSO and LSO congruently melting crystals are usually grown by the Czochralski method. Oxyorthosilicates are ready to form solid solutions which allow the reduction of both growing temperature and raw material cost. $Lu_xY_{2-x}SiO_5$ (LYSO) or $Lu_xGd_{2-x}SiO_5$ (LGSO) crystals prepared by partially replacing Lu^{3+} ions by larger Y^{3+} or Gd^{3+} ions adopt to the *C2/c* (LSO) type structure [7,8]. For scintillator applications the rare earth ionic fraction, *x* determines the performance, since Y/Gd substitution proportionally increases the unit cell volume and decreases the crystal density, thereby affecting the scintillation efficiency.

The optical properties of monoclinic crystals are anisotropic. The biaxial character of oxyorthosilicates is rarely considered in scintillator applications, since birefringence is irrelevant considering light output properties of the crystal. However, for laser studies and consistent spectroscopic evaluation of the crystal properties, the knowledge of the direction-dependent refractive indices is required. The biaxial character of wavelength-dependent parameters is also to be taken into account in simulations of absorption and scattering loss. These parameters are usually determined from the measured transmittance of the sample, the direction-dependent refractive index of which should be known so that transmission data can be properly corrected for reflection at the crystal-air interfaces [9].

For monoclinic crystals such as LYSO, only one of the three orthogonal principal axes of the optical indicatrix is collinear with the 2-fold crystallographic *b* axis and the other two lay in the (0 1 0) plane. The directions of these latter do not necessarily coincide with the crystallographic axes and may vary with the wavelength – a phenomenon called *dispersion of axes* [10]. For transparent materials the axial dispersion is usually small in the visible range with a large band gap, however for certain monoclinic and triclinic crystals the effect is measurable and may have practical importance. The refractive indices of LSO and LYSO crystals were measured by the V-prism method at four different wavelengths neglecting the birefringence properties of the crystal [11]. The relative orientation of the optical indicatrix axes and the crystallographic axes ***a***, ***c*** (in *I2/a* setting) has been determined by polarization microscopy for Er-Yb-doped YSO crystal [12]. The dispersion coefficients for the principal refractive indices of the Nd-doped YSO crystal was deduced from minimum-deviation angle measurements in the wavelength range of 435.8–643.8 nm [13].

* Corresponding author.
E-mail address: lorincz@eik.bme.hu (E. Lőrincz).

0925-3467/$ - see front matter © 2011 Elsevier B.V. All rights reserved.
doi:10.1016/j.optmat.2011.11.006

The purpose of the present communication is to precisely determine the wavelength dependence of the missing principal refractive indices of the biaxial LYSO crystal. For biaxial crystals, such as LYSO, the axial dispersion has an influence on the refractive index, as a result of which the optical indicatrix rotates around the crystallographic ***b*** axis as a function of the wavelength. In order to estimate the effect of the axial dispersion, the variation of the polarization extinction angle in (0 1 0)-cut LYSO samples was measured for the wavelength range of 250–900 nm. Finally, we give two examples to quantify the effects of anisotropy on the operation of optical devices.

2. Experimental details

2.1. Sample preparation

Crystal prisms were prepared from a LYSO:Ce crystal grown by the Czochralski technique (produced by Sinoceramics, Incorporation, Shanghai, China). The nominal Ce concentration of the crystal was 0.2 at%. The lattice parameters of the crystal boule were determined by X-ray powder diffraction analysis. The obtained cell parameters in *C2/c* setting are $a = 14.298(1)$ Å, $b = 6.663(3)$ Å, $c = 10.280(1)$ Å, $\beta = 122^\circ 20'$, $V = 827.538$ Å^3. A lutetium content of $x = 1.6$ was determined from the cell volume by using the Vegard's rule. The crystallographic orientation of the samples was determined by X-ray diffraction, while directions of the optical indicatrix axes (***X***, ***Y***, ***Z*** with the setting $n_x < n_y < n_z$) were determined by means of polarized light microscopy (see Fig. 1). Rotating a polished (0 1 0) (*b*-cut) crystal in white light between crossed polarizers the extinction positions could be well determined indicating a low angular dispersion in the visible range. Accordingly, the ***X*** indicatrix axis coincides with the 2-fold *b* axis and the acute bisectrix (***Z*** axis) is close to the normal of the $(-1\,0\,2)$ plane.

For optical refractive index measurements triangular-prisms were prepared with an apex angle of about 54° and base normal parallel with one of the indicatrix axis. Refracting surfaces were prepared by mechanical polishing, finished with 0.1 μm grain sized diamond paste. Prisms were prepared in *YX*, *XY*, *ZY* and *YZ* orientations, allowing for the determination of (n_y, n_z), (n_x, n_z), (n_z, n_x) and (n_y, n_x) refractive indices, respectively. Here the prism orientation is denoted by a two-letter code (*YX*), where the letters correspond to the normal vector orientations of the prism's base and symmetry plane, respectively. In the case of minimum deflection angle (δ), the second direction is parallel to the light beam inside the prism (see Fig. 2). In our measurements the prism's base was always precisely set parallel to the plane of light deflection. The error in the optical indicatrix axis orientation (***X***, ***Y***, ***Z***) relative to the prism sides was smaller than 0.5°. The apex angles of the prisms were measured with a precision of ±0.01°.

2.2. Measuring equipment for refractive index

For refractive index measurement a goniometer (made by Freiberger Präzisionsmechanik) was used with an angular resolution of two arc seconds. The original tungsten lamp of the collimator unit was replaced by a custom light source, in which we used color LEDs operated independently to map the wavelength dependence of the refractive index. In order to further reduce the spectral bandwidth, we applied interchangeable interference filters in the light source, with transmission curves centered to the peak wavelengths of the LEDs. The measured emissions spectra of our light source for 409, 470, 481, 524, 590, 631, 670 nm central wavelengths are shown in Fig. 3. The spectral width is 10–11 nm FWHM. The LED light source was unpolarized, thus each measurement resulted in two orthogonally polarized light beams of different δ values (see Fig. 2). We used a Glan–Thompson polarizer to identify the polarization direction of the beams.

2.3. Measuring equipment for axial dispersion

In order to measure axial dispersion we prepared a LYSO sample in the form of a plane-parallel plate with 1.0 mm thickness and polished surfaces. This sample was oriented in (0 1 0) direction so that the crystallographic ***b*** axis (and correspondingly the ***X*** indicatrix axis) was *orthogonal* to the surface planes. For the measurement we used a SEMILAB GES-5E ellipsometer with its illumination and detector arms both aligned horizontally, opposite to each other. The sample was put in between the two arms with its plane surfaces orthogonal (and thus the ***b***-axis parallel) to the incident light beam. The polarizer and the analyzer of the ellipsometer were set orthogonally to each other, thus the sample was always examined between two crossed polarizers. The aligned analyzer-polarizer pair was rotated 180° around the light beam by 2° step intervals. At each angular position the transmission (T) of the polarizer-sample-analyzer assembly was recorded for the entire spectrum from 250 to 900 nm. The transmission is expected to be sinusoidal as a function of the polarizer angle (φ):

$$T(\lambda) = A(\lambda) \cdot \sin^2(\varphi + \varphi_0(\lambda)) + T_0(\lambda). \quad (1)$$

In the above equation $A(\lambda)$ denotes the amplitude, $T_0(\lambda)$ is an offset value near zero, $\varphi_0(\lambda)$ is the starting phase and λ is the wavelength. The transmission minima indicate the angles where the polarizer is

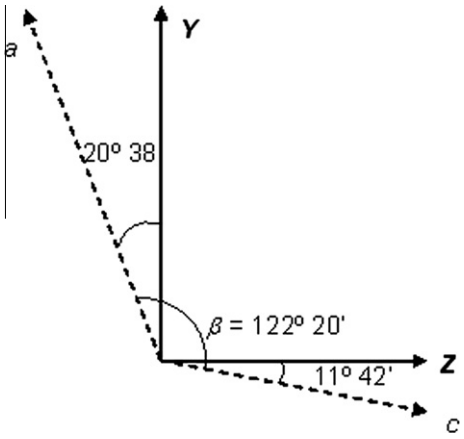

Fig. 1. Orientation of the optical indicatrix axes ***Y*** and ***Z*** in the C2/c setting. Symbols *a* and *c* indicate crystal axes.

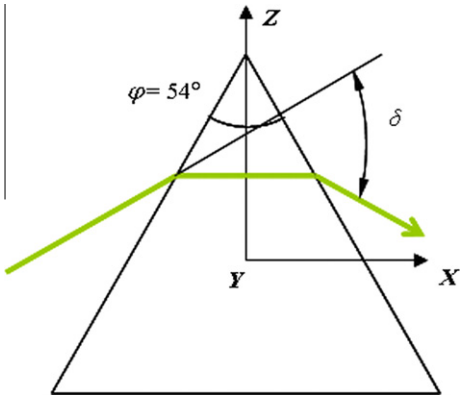

Fig. 2. Triangular-prism prepared in *YX* orientation for the measurement of n_y and n_z refractive indices. A sample light beam is indicated with a minimum deflection angle δ. See details in the text.

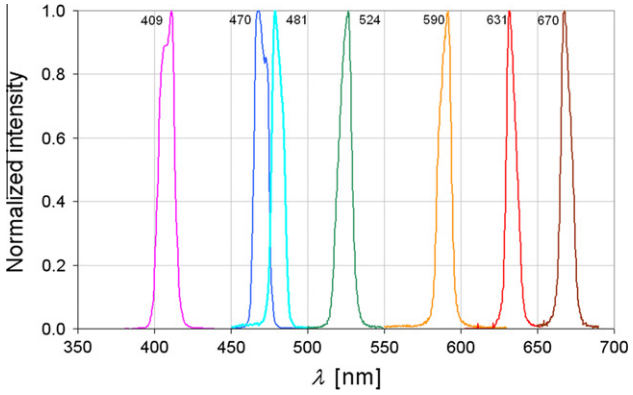

Fig. 3. Measured power spectral density of the filtered LED sources. Values are normalized to unity.

aligned with one of the optical indicatrix principal axes. Indeed, in such cases the incoming linearly polarized light does not suffer any change in its polarization state, thus the orthogonally set analyzer absorbs almost all the light coming through the sample. Using appropriate software tools we determined the above parameters by fitting (1) to the measured experimental transmission curves. The values of $A(\lambda)$ and $T_0(\lambda)$ have no significance here. It is only the starting phase $\varphi_0(\lambda)$ that determines the angular positions of the minima and thus the direction of the indicatrix principal axis at each wavelength.

3. Results and discussion

Table 1 shows the measured average values and standard deviations of the principal indices of refraction at seven different wavelengths for the above mentioned orientations *YX*, *XY*, *ZY* and *YZ*. LYSO is found optically biaxial positive: at $\lambda = 524$ nm the angle between the two optical axes is $2V_z = 22.45^\circ$ and principal refractive indices are $n_x = 1.8077$, $n_y = 1.8110$ and $n_z = 1.8307$.

The wavelength-dependent principal refractive indices were fit by the method of least squares to a modification of Sellmeier's dispersion formula [12,14], commonly used for crystals:

$$n_i^2 = A + \frac{B}{\lambda^2 + C} + D\lambda^2, \quad i = x, y, z \tag{2}$$

where λ is the wavelength in microns and n_i is the principal refractive index of interest. The coefficients for the best fit case are given in Table 2.

By using the dispersion coefficients given in Table 2 the difference between the measured and calculated principal indices are less than ±0.0001. Fig. 4 shows the calculated dispersion curves of LYSO extrapolated towards the infrared wavelengths together with the measured values and the results published in Ref. [11].

3.1. Crystallographic considerations

The dispersion curves of n_x and n_y principal indices run practically together (Fig. 4.), the minor difference in their values may explain the different assignment of the *X*-axis published by other authors [12,15]. Similarly to the results of Beach et al. on Nd-doped YSO [12], we found the ***X*** axis to be parallel to the 2-fold ***b*** axis. For Yb-doped YSO and LSO crystals the ***b*** axis has been reported to be parallel with the ***Y*** indicatrix axis [15] meaning that in these crystals the optical plane containing the directions corresponding to the lower refractive and larger indices ***X*** and ***Z*** is the (010) plane. The diverse assignment of the orientation of ***X*** axis may be related to the RE doping of the lattice, since the LSO unit cell contains two

Table 1
Measured and averaged principal indices of LYSO prisms for each wavelength.

λ(nm)	–	n_x	n_y	n_z
409	*YX*	–	1.8312	1.8524
	XY	1.8280	–	1.8525
	ZY	1.8276	–	1.8523
	YZ	1.8276	1.8315	–
		1.8277±0.0002	**1.8313±0.0004**	**1.8524±0.0001**
470	*YX*	–	1.8186	1.8389
	XY	1.8153	–	1.8389
	ZY	1.8149	–	1.8385
	YZ	1.8155	1.8187	–
		1.8152±0.0003	**1.8186±0.0002**	**1.8388±0.0002**
481	*YX*	–	1.8167	1.8370
	XY	1.8136	–	1.8371
	ZY	1.8133	–	1.8369
	YZ	–	–	–
		1.8135±0.0003	**1.8167**	**1.8370±0.0001**
524	*YX*	–	1.8042	1.8237
	XY	1.8077	–	1.8309
	ZY	1.8074	–	1.8306
	YZ	1.8079	1.8112	–
		1.8077±0.0002	**1.8110±0.0003**	**1.8307±0.0001**
590	*YX*	–	1.8042	1.8237
	XY	1.8010	–	1.8236
	ZY	1.8017	–	1.8235
	YZ	1.8014	1.8045	–
		1.8014±0.0004	**1.8044±0.0003**	**1.8236±0.0001**
631	*YX*	–	1.8012	1.8206
	XY	1.7983	–	1.8206
	ZY	1.7982	–	1.8204
	YZ	1.7981	1.8016	–
		1.7982±0.0001	**1.8014±0.0004**	**1.8205±0.0001**
670	*YX*	–	1.7990	1.8182
	XY	1.7958	–	1.8180
	ZY	1.7957	–	1.8181
	YZ	1.7959	1.7994	–
		1.7958±0.0001	**1.7992±0.0004**	**1.8181±0.0001**
670	*YX*	–	1.7990	1.8182
	XY	1.7958	–	1.8180
	ZY	1.7957	–	1.8181
	YZ	1.7959	1.7994	–
		1.7958±0.0001	**1.7992±0.0004**	**1.8181±0.0001**

Table 2
Dispersion coefficients for the principal refractive indices of LYSO.

	n_x	n_y	n_z
A (–)	3.1645	3.172	3.236
B (μm^2)	0.0276	0.0287	0.03034
C (μm^2)	−0.0114	−0.0093	−0.0118
D (μm^{-2})	−0.0055	−0.0015	−0.0005

different RE^{3+} sites (Lu1, Lu2), coordinated by six and seven O atoms, respectively. The yttrium incorporation into the LSO lattice, in analogy with Ce, was found preferentially at the larger 7-coordinated Lu2 sites. The coordination polihedra of RE1 and RE2 ions are linked in interpenetrating frameworks forming compact chains along the ***b*** axis. Incorporation of RE ions of larger ionic radius, like Nd^{3+}, Ce^{3+} into the lattice increases the structural deformation involving the modifications of optical properties.

3.2. The effect of axial dispersion on refractive index

The wavelength dependence of the orientation of the ***Y*** and ***Z*** optical indicatrix axes is summarized in Fig. 5. It can be seen that the axes really rotate approximately 8° in the total measured, and 2.4° in the 400–700 nm spectral range which is of importance in scintillator applications. In the following we estimate the refractive index error (Δn) caused by neglecting axial dispersion. Let us assume that optical indicatrix of a LYSO scintillator crystal was

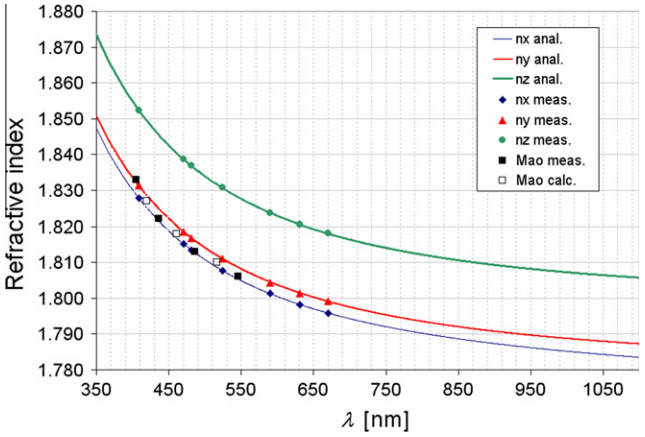

Fig. 4. Dispersion curves of the principal refractive indices of LYSO calculated by the formula (1) and coefficients of Table 2. Measured values of the indices and the results of Mao [11] are also plotted.

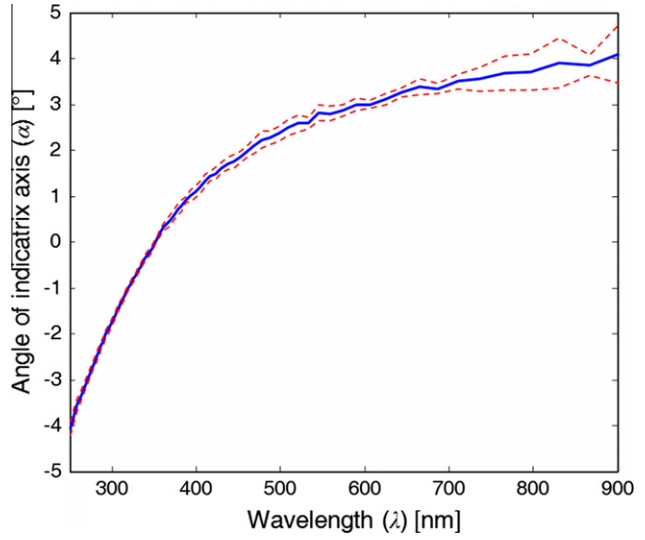

Fig. 5. Dispersion of polarization extinction angle within the (010) plane (the $\alpha = 0$ point position has been selected arbitrarily). Dashed line shows standard deviation of the measurement.

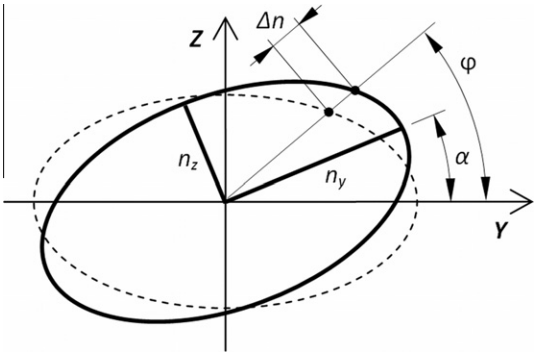

Fig. 6. Explanation for calculating the effect of neglecting axial dispersion on refractive index. Solid line indicates real indicatrix position at a given wavelength, dashed line shows the same in case of axial dispersion neglected. The angle φ denotes actual polarization direction of incident light. See details in the text.

oriented using $\lambda = 500$ nm light, around which the amount of axial dispersion is symmetric in the 400–700 nm range (±1.2°). In this case we obtain the largest error when a collimated beam of light travels through the crystal parallel to the ***X***-direction at a wavelength far from 500 nm. Since the difference of n_z and n_y grows

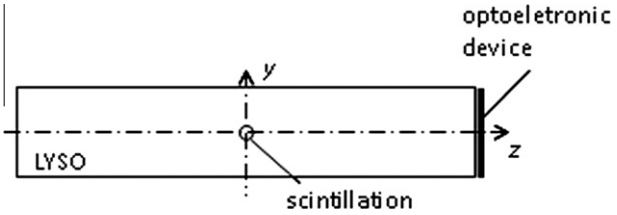

Fig. 7. Scheme of the scintillation detector applied in our example.

with shorter wavelengths, we consider $\lambda = 400$ nm to determine the maximum error. At this wavelength $n_y = 1.8338$ and $n_z = 1.8550$, and the rotation of indicatrix axes is $\alpha = -1.2°$, according to Fig. 6. By rotating the polarization vector of incident light in the ***Y–Z*** plane we calculated the difference of refractive index (Δn) between a rotated (n') and a non-rotated indicatrix (n), see Fig. 6. Since n_y and n_z are close to each other, and α is very small, an approximative analytical expression can be derived for Δn as the polarization of the incoming light rotates around. Using the ellipse equation in polar coordinates, the refractive index difference is:

$$\Delta n \approx \underbrace{\sqrt{(n_y \sin(\varphi-\alpha))^2 + (n_z \cos(\varphi-\alpha))^2}}_{n} - \underbrace{\sqrt{(n_y \sin(\varphi))^2 + (n_z \cos(\varphi))^2}}_{n'}, \tag{3}$$

where φ denotes the polarization direction of the incident light. Please note that Eq. (3) is an approximation. It is only valid for cases when $n_y \approx n_z$. Since $\alpha << 1$ [rad] the following linear approximations can be made (angles are considered in radians from now on):

$$\begin{aligned} \sin^2(\varphi-\alpha) &\approx \sin^2(\varphi) - \sin(2\varphi)\cdot\alpha; \\ \cos^2(\varphi-\alpha) &\approx \cos^2(\varphi) + \sin(2\varphi)\cdot\alpha. \end{aligned} \tag{4}$$

Using the above, the first term in (3) will be:

$$n \approx \sqrt{(n_y \sin(\varphi))^2 + (n_z \cos(\varphi))^2} \cdot \sqrt{1 + \frac{(n_z^2 - n_y^2)\cdot\sin(2\varphi)\cdot\alpha}{(n_y \sin(\varphi))^2 + (n_z \cos(\varphi))^2}}. \tag{5}$$

Applying a Taylor series-expansion for the square root (5) can be further approximated:

$$n \approx \sqrt{(n_y \sin(\varphi))^2 + (n_z \cos(\varphi))^2} \cdot \left[1 + \frac{1}{2}\cdot\frac{(n_z^2 - n_y^2)\cdot\sin(2\varphi)\cdot\alpha}{(n_y \sin(\varphi))^2 + (n_z \cos(\varphi))^2}\right]. \tag{6}$$

Substituting (6) into (3) we get the final result:

$$\begin{aligned} \Delta n &\approx \frac{1}{2}\cdot\frac{(n_z^2 - n_y^2)\cdot\sin(2\varphi)\cdot\alpha}{\sqrt{(n_y \sin(\varphi))^2 + (n_z \cos(\varphi))^2}} \\ &\approx \frac{(n_z^2 - n_y^2)\cdot\alpha}{n_z + n_y}\cdot\sin(2\varphi), \end{aligned} \tag{7}$$

where we approximated the denominator by the average refractive index. Note that the unit of α is radian.

According to (7), the amplitude, i.e. the maximum value of the refractive index error is $\Delta n_{max} = 4.4 \times 10^{-4}$. (The above approximations cause less than $\pm 10^{-5}$ uncertainty in this value.) In consequence, in models where axial dispersion is neglected, the refractive index measurement error must be supplemented with the above value. Since our measurement precision was 0.0005, the resulting error is ±0.001 in the range of 400–700 nm. It must

be noted that this is the standard refractive index error of commercial optical glasses.

3.3. Application examples from optics

In order to illustrate the effects of anisotropic refractive index on the operation of optical devices, two examples will be presented. First, we consider the case of a simple plane-parallel plate of crystalline LYSO with polished surfaces. Below, we determine in what extent the crystal anisotropy (i.e. direction- and polarization-dependence of its refractive index) influences the power transmission (T') of the above described LYSO slab. Due to Fresnel reflection there is always a loss when light transmits a boundary of materials with different refractive indices. The amount of light transmitted is determined by the refractive index of the two materials. Since there are multiple reflections on the parallel surfaces, the transmission of the slab can only be written in the form of an infinite series. Using linearly polarized light and assuming no absorption and no interference, the sum of the series will result in [16]:

$$T' = 1 - \frac{2R}{R+1}, \tag{8}$$

where R denotes the surface reflection. For normal incidence:

$$R = \left[\frac{n_i - 1}{n_i + 1}\right]^2, \tag{9}$$

where the $i = x, y, z$ index shows the optical indicatrix axis along which the incident light is polarized. Results are summarized in Table 3 for 524 nm wavelength. We calculated (8) and (9) using the refractive indices in Table 1. The effect of anisotropy is not large, however clearly observable.

Our second example illustrates a more complex case taken from the field of PET (Positron Emission Tomography) detectors. The basis of explanation is again Fresnel reflection. Now we regard a simplified arrangement of human PET detectors: it consists of a LYSO scintillation crystal to convert gamma-radiation into visible light, and an optoelectronic device (e.g. photoelectron multiplier) to capture the visible photons. In order to exclude disturbing effects of special components, we take into account only the simplest possible detector configuration: $4.0 \times 4.0 \times 20.0$ mm crystal with polished surfaces (no coating). The optoelectronic device is rectangular, matching the size of the crystal, and is fitted to the scintillator end with a small (0.1 mm) air–gap in between. The arrangement is outlined in Fig. 7.

The scintillation takes place at the center of the crystal. Unpolarized light is assumed to emanate from a spherical volume of 0.2 mm diameter. The wavelength-dependent emission and absorption spectra [17] as well as the refractive index of LYSO are taken into account. For the simulation we used the ZEMAX commercial optical design software [18] in non-sequential ray-tracing mode. Since the software can handle only uniaxial birefringence, anisotropy of LYSO was approximated by the following: $n_{ordinary} \approx n_x$ and $n_{extraordinary} \approx n_z$. Average and standard deviation of the ratio of detected photons to the launched photons in one scintillation (light output) have been calculated for four scintillation events. Results are listed in Table 4.

Table 3
Orientation-dependent transmission (T') of a plane-parallel plate of LYSO at orthogonal incidence ($\lambda = 524$ nm, linear polarization). See details in the text.

	n_i (–)	R (%)	T (%)
x	1.8077	8.27	84.71
y	1.811	8.32	84.63
z	1.8307	8.61	84.14

Table 4
Light output in a PET detector using anisotropic LYSO scintillator crystal.

Crystal axis orientation	Average light output	Standard deviation
Isotropic case ($n = n_{ordinary}$)	16.05%	±0.05%
Aligned with Y-axis	15.96%	±0.02%
Aligned with Z-axis	15.88%	±0.03%

From our results it can be seen that the anisotropy has indeed a minor effect on the light output of the PET detectors. According to our experience, other parameters such as surface roughness affect light yield in a much larger extent.

4. Conclusions

Principal refractive indices of single crystalline LYSO were determined in the wavelength range of 400–700 nm by the minimum angle of deviation method using sample prisms with different crystallographic orientations. Standard deviation of the results was less than 0.0005 for all wavelengths. Axial dispersion of the optical indicatrix was found to be in the range of the experimental error. If axial dispersion is neglected, the error in the refractive index in the visible wavelength range increases to 0.001. The calculated dispersion coefficients allow for an extrapolation of the principal indices to an extended wavelength range of 350–1100 nm. For any wavelength the difference between n_y and n_x is less than 0.0004 that is smaller than our measurement error. As an application of the results we pointed out that refractive index anisotropy has a negligible effect on the calculated light output of a scintillator crystals made from LYSO. However, for accurate determination of the reflection loss at the crystal surfaces the anisotropy has to be taken into consideration.

Acknowledgements

The authors wish to thank to Mediso Ltd. for providing the LYSO crystal, Gy. Matók and A. Chalupa for the sample preparation. This work was supported by the Hungarian Scientific Research Fund (OTKA) Nos. CK 80892 and CK 80896 and NHDP TÁMOP-4.2.1/B-09/1/KMR-2010-0002.

References

[1] J. Chen, L. Zhang, R. Zhu, Nucl. Instrum. Methods Phys. Res. A 572 (2007) 218.
[2] D.W. Cooke, R.E. Muenchausen, K.J. McClellan, B.L. Bennett, Opt. Mater. 27 (2005) 1781.
[3] W. Li, S. Xu, H. Pan, L. Ding, H. Zeng, W. Lu, C. Guo, G. Zhao, C. Yan, L. Su, J. Xu, Opt. Express 14 (15) (2006) 6681.
[4] F. Thibault, D. Pelenc, F. Druon, Y. Zaouter, M. Jacquemet, P. Georges, Opt. Lett. 31 (2006) 1555.
[5] Wenxue Li, Qiang Hao, Hui Zhai, Heping Zeng, Wei Lu, Guangjun Zhao, Lihe Zheng, Liangbi Su, Jun Xu, Opt. Express 15 (2007) 2354.
[6] J. Felsche, in: J.D. Dunitz (Ed.), In Structure and Bonding, vol. 13, Springer-Verlag, Berlin, 1973, p. 99.
[7] D. Chiriu, N. Faedda, A.G. Lehmann, P.C. Ricci, A. Anedda, S. Desgreniers, E. Fortin, Phys. Rev. B76 (2007) 054112.
[8] G. Dominiak-Dzik, W. Ryba-Romanowski, R. Lisiecki, P. Solarz, B. Macalik, M. Berkowski, M. Glowacki, V. Domukhovski, Cryst. Growth Des. 10 (2010) 3522.
[9] D.J. van der Laan, D.R. Schaart, M.C. Maas, F.J. Beekman, P. Bruyndonckx, C.W.E. van Eijk, Phys. Med. Biol. 55 (2010) 1659.
[10] M. Born, E. Wolf, Principles of Optics, 6th ed., Pergamon Press, 1991.
[11] R. Mao, L. Zhang, R-Y. Zhu, IEEE Trans. Nucl. Sci. 55 (4) (2008) 2425.
[12] C. Li, C. Wyon, R. Moncorgé, IEEE J. Quantum Electron. 28 (1992) 1209.
[13] R. Beach, G. Albrecht, R. Solarz, W. Krupke, B. Comaskey, S. Mitchell, C. Brandle, G. Berkstresser, Proc. SPIE 1223 Solid State Lasers 160 (1990).
[14] Handbook of Optics, vol. II, McGraw-Hill, 1995, pp. 33.61.
[15] M. Jacquemet, C. Jacquemet, N. Janel, F. Druon, F. Balembois, P. Georges, J. Petit, B. Viana, D. Vivien, B. Ferrand, Appl. Phys. B 80 (2005) 171.
[16] Handbook of Optics, vol. I, McGraw-Hill, 1995, pp. 5.16.
[17] E. Lőrincz, G. Erdei, I. Péczeli, C. Steinbach, F. Ujhelyi, T. Bükki, IEEE Trans. Nucl. Sci. 57 (1) (2010) 48.
[18] ZEMAX: Software For Optical System Design, <http://www.zemax.com/>.